J. Phys.: Condens. Matter **22** (2010) 015004 (11pp) doi:10.1088/0953-8984/22/1/015004

Ab initio structure modelling of complex thin-film oxides: thermodynamical stability of TiC/thin-film alumina

J Rohrer[1], **C Ruberto**[1,2] **and P Hyldgaard**[1]

[1] BioNano Systems Laboratory, Department of Microtechnology, MC2, Chalmers University of Technology, SE-412 96 Gothenburg, Sweden
[2] Materials and Surface Theory Group, Department of Applied Physics, Chalmers University of Technology, SE-412 96 Gothenburg, Sweden

E-mail: rohrer@chalmers.se

Received 7 October 2009, in final form 8 October 2009
Published 3 December 2009
Online at stacks.iop.org/JPhysCM/22/015004

Abstract
We present a strategy to identify energetically favourable oxide structures in thin-film geometries. Thin-film candidate configurations are constructed from a pool of sublattices of stable and metastable oxide bulk phases. Favourable stoichiometric compositions and atomic geometries are identified by comparing total and Gibbs free energies of the relaxed configurations. This strategy is illustrated for thin-film alumina on TiC, materials which are commonly fabricated by chemical vapour deposition (CVD) and used as wear-resistant multilayer coatings. Based on the standard implementation of *ab initio* thermodynamics, with an assumption of equilibrium between molecular O_2 and the oxide, we predict a stability preference of TiC/alumina configurations that show no binding across the interface. This result is seemingly in conflict with the wear-resistant character of the material and points towards a need for extending standard *ab initio* thermodynamics to account for relevant growth environments.

Supplementary data are available from stacks.iop.org/JPhysCM/22/015004/mmedia

1. Introduction

Understanding the atomic and electronic structure of thin-film oxides is of significant industrial and fundamental importance and a huge challenge at the same time. Bulk oxides are characterized by a strong ionicity, which often results in a tendency for high structural flexibility and organization in a large number of different stable and metastable phases. Prominent examples can be found among aluminium oxides[3], titanium oxides[4], vanadium oxides[5] or hafnium oxides[6]. For an ultra-thin film, the structural variety of the oxide can be even larger [5, 6]. The mainly insulating character of oxides makes accurate experimental atomic and electronic structure determinations difficult, since high-resolution techniques (low energy electron diffraction (LEED) [5], scanning tunnelling microscopy (STM) [6], transmission electron microscopy (TEM) [7], scanning electron microscopy(SEM) [8], etc) mainly use charged particles. Theory-assisted methods, such as density functional theory (DFT) calculations, are of high complementary value. However, when modelling thin films that are adsorbed on a substrate, relatively large surface unit cells are often needed. As a consequence, an enormous number of possible atomic configurations for the film arises and a structure determination by straightforward energy calculations of all possible candidates becomes computationally intractable.

The nucleation of alumina on TiC provides an illustration of the complexity and importance of predicting and understanding the atomic structure in oxides, ultra-thin oxide films and their interfaces. Multilayers of TiC, α-Al_2O_3 and κ-Al_2O_3 are highly relevant for industrial application as wear-resistant coatings on cemented-carbide cutting tools [9].

[3] α-, γ-, δ-, θ-, κ-Al_2O_3, ..., see, e.g., Levin and Brandon [1].
[4] Rutile-, anatase-, brookite and columbite (α-PbO_2) TiO_2 and Ti_2O_3, see, e.g., Haines and Leger [2].
[5] VO_x (rocksalt), VO_2 (rutile), V_2O_3 (corundum) and V_2O_5 (orthorhombic), see, e.g., Surnev *et al* [3].
[6] Cubic, tetragonal and monoclinic modifications of HfO_2, see, e.g., Wang *et al* [4].

 © 2010 IOP Publishing Ltd Printed in the UK

However, these ordered structures only arise when the alumina possesses a considerable thickness. The nucleation of alumina on TiC involves the formation of ultra-thin alumina films. Insight into the detailed atomic configuration in the ultra-thin films is essential because their structure may strongly influence the subsequent growth [10]. A complete search through all possible atomic thin-film configurations by total energy calculations is, however, extremely difficult[7].

In this paper, we propose an, in principle, general and computationally more realizable *ab initio* strategy to search for favourable geometries of thin-film oxides on metallic surfaces. We illustrate the strategy for TiC/thin-film alumina. First, a pool of promising thin-film candidates with different thicknesses and stoichiometric compositions is created from the structural motifs of the sublattices of stable and metastable alumina bulk phases. We then use DFT calculations to relax the combined configurations consisting of the substrate and the thin-film candidates. We order the relaxed configurations by means of their Gibbs free energies calculated in the framework of *ab initio* thermodynamics [11–13], identify the characteristics of the structural motifs of the relaxed films and discuss these as well as the nature of the binding across the interface. This procedure could then be iterated until self-consistency is reached, that is, the favourable motifs of the relaxed films can be used to broaden the pool from which thin-film candidates are constructed (and the process is iterated until the relaxed films do not contain motifs that are not already included in the pool of structurally favourable motifs).

This paper is organized as follows: section 2 summarizes the properties of alumina and TiC that are relevant for TiC/thin-film alumina. In section 3 we derive all TiC/thin-film alumina initial configurations that are consistent with the bulk structure of the respective materials. The details concerned with the computation of total and Gibbs free energies are discussed in section 4. In section 5, we present our results on the energetics and thermodynamical stability of thin-film alumina as well as an analysis of the atomic structure of relaxed films. In section 6, we discuss our results and section 7 contains our conclusions.

2. Materials background

TiC/alumina multilayers are commonly fabricated by chemical vapour deposition (CVD). Typically, the α-Al_2O_3 (stable in the bulk) and κ-Al_2O_3 (metastable in the bulk) phases are obtained with relative orientations of $\alpha(0001) \parallel$ TiC(111) and $\kappa\{001\} \parallel$ TiC(111) [14].

2.1. Stable and metastable Al_2O_3 bulk structures

Figure 1 details the bulk structures of α-Al_2O_3 (trigonal unit cell, space group $R\bar{3}c$, here displayed in an orthorhombic unit cell, with $\alpha[0001]_{hex} \Leftrightarrow \alpha[001]_{ortho}$, to facilitate a parallel treatment with κ-Al_2O_3; in the following, the subscript label is dropped) and κ-Al_2O_3 (orthorhombic unit cell, space group $Pna2_1$) [15, 16]. The associated calculated lattice parameters are $a = 4.798$ (4.875) Å, $b = 8.311$ (8.378) Å and $c = 13.149$ (9.018) Å for α (κ) [17, 16], which is in good agreement with experimental data [18, 19].

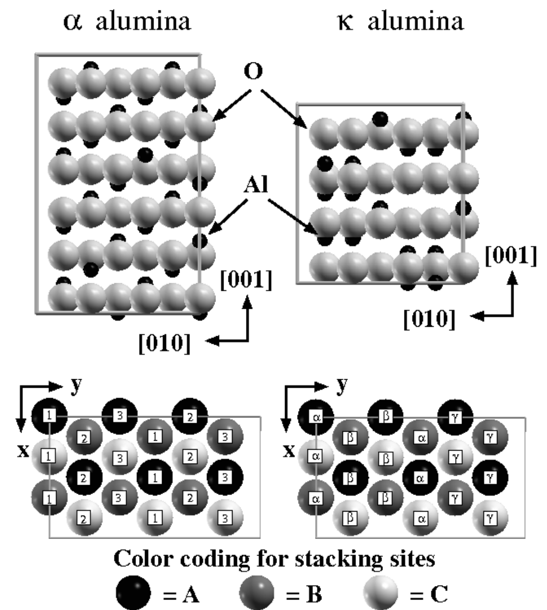

Figure 1. Bulk structures of α- (left) and κ-Al_2O_3 (right) within orthorhombic unit cells. The top panels show side views along [100]. The bottom panels define the atomic site labelling within each (001) atomic layer.

Along the $\alpha[0001]$ and $\kappa[001]$ directions, both alumina phases are composed of alternating O and Al layers, the latter splitting up into two sublayers. In α-Al_2O_3, all Al ions are octahedrally (O) coordinated. In κ-Al_2O_3, the coordination alternates. In every second layer all Al ions have octahedral coordination. In the other layers 50% of the Al ions are octahedrally and 50% tetrahedrally (T) coordinated. All tetrahedra point in the [001] direction.

The stacking along the [001] directions of α- and κ-Al_2O_3 can be described as [20, 16]

$$\begin{aligned} \alpha[001]&: Ac_3c_2Bc_1c_3Ac_2c_1Bc_3c_2Ac_1c_3Bc_2c_1 \\ \kappa[001]&: Ab_\gamma c_\beta Bc_\alpha c_\gamma Ac_\beta b_\gamma Cb_\alpha b_\beta . \end{aligned} \quad (1)$$

Here, we have denoted the stacking sites of full O layers by capital letters. For Al layers lower-case letters with a subscript (Arabic numerals for α-, Greek letters for κ) are used. The subscript each relates to two Al sites per unit cell, see the lower panel in figure 1 for a detailed definition of each label. For κ this notation is identical to the one introduced in [16], whereas for α it is a slightly modified version of the one in [20], where Greek superscripts are used for the labelling of Al vacancies.

2.2. TiC(111) surface and reactivity

Bulk TiC possesses a NaCl structure. It is composed of close-packed alternating Ti and C layers with $ABCABC$ stacking

[7] Both alumina phases, in particular κ-Al_2O_3, yield a huge number of possible thin-film configurations. The primitive unit cell of κ-Al_2O_3, with its $ABAC$ stacking of O planes along the [001] direction, see also figure 1, allows for $\binom{18}{4} = 3060$ combinatorially possible distributions of the four Al ions within each atomic plane. Use of symmetry and electrostatics arguments (for example, no occupation of nearest-neighbour sites for Al) reduces this number to 222. However, it is clear that, for thin films of a few atomic layers, the number of possible atomic structures increases rapidly.

Table 1. TiC(111)/alumina interface configurations that respect the bulk structure of α- and κ-Al_2O_3 and start with an O layer in the fcc site on the Ti-terminated TiC(111). The TiC stacking of the surface region is defined as $\ldots ABCABC$.

TiC/α[0001]	TiC/κ[001]	TiC/κ[00$\bar{1}$]
TiC/$Ac_3c_2Bc_1c_3Ac_2c_1Bc_3c_2Ac_1c_3Bc_2c_1$	TiC/$Ab_\gamma c_\beta Bc_\alpha c_\gamma Ac_\beta b_\gamma Cb_\alpha b_\beta$	TiC/$Ab_\beta b_\alpha Cb_\gamma c_\beta Ac_\gamma c_\alpha Bc_\beta b_\gamma$
TiC/$Ab_2b_3Cb_1b_2Ab_3b_1Cb_2b_3Ab_1b_2Cb_3b_1$	TiC/$Ab_\alpha b_\gamma Cb_\beta a_\gamma Ba_\alpha a_\beta Ca_\gamma b_\beta$	TiC/$Ab_\beta a_\gamma Ca_\beta a_\alpha Ba_\gamma b_\beta Cb_\gamma b_\alpha$
	TiC/$Ac_\beta b_\gamma Cb_\alpha b_\beta Ab_\gamma c_\beta Bc_\alpha c_\gamma$	TiC/$Ac_\gamma c_\alpha Bc_\beta b_\gamma Ab_\beta b_\alpha Cb_\gamma c_\beta$
	TiC/$Ac_\alpha c_\beta Bc_\gamma a_\beta Ca_\alpha a_\gamma Ba_\beta c_\gamma$	TiC/$Ac_\gamma a_\beta Ba_\gamma a_\alpha Ca_\beta c_\gamma Bc_\beta c_\alpha$

(for one repeat unit) along the [111] direction. The calculated lattice parameter is $a = 4.332$ Å [21] and in good agreement with the experimental value $a_{exp} = 4.33$ Å [22].

We only consider Ti-terminated TiC(111) surfaces. This choice is motivated by the stronger binding of Ti to the C-terminated surface compared to the binding of C to the Ti-terminated surface [21]. Furthermore, there is experimental evidence for a preferred Ti termination upon annealing [23].

On Ti-terminated TiC(111), atomic O adsorbs much more strongly than atomic Al (about three times as strong) [21]. We therefore identify the first alumina layer above the TiC/Al_2O_3 interface plane as an O layer. According to [21] and [7], both single O atoms and a full O monolayer prefer adsorption on the fcc site. By defining the TiC stacking such that the fcc site on its (111) surface is labelled by an A stacking letter, the hcp site by B and the top site by C, the position of the first O layer is therefore fixed to A stacking. For the monolayer, our calculated Ti–O layer separation along TiC[111] is $d_{Ti-O} = 0.89$ Å.

3. Thin-film identification strategy

The strategy that we pursue for identifying low energy geometries for alumina on TiC consists of two parts. First, we determine all TiC/alumina interface configurations that are consistent with the α- and κ-Al_2O_3 bulk structures and that take into account the adsorption properties of the TiC(111) surface. Then, we obtain all initial thin-film candidates that consist of structural motifs of bulk alumina by truncating the interface sequences in different ways and allowing for various stoichiometric compositions.

3.1. TiC/alumina interface structures

Table 1 lists all TiC/alumina interface sequences that conform with the α- and κ-Al_2O_3 bulk structures and that start with an O layer in the fcc (A) site on the Ti-terminated TiC(111) surface. These stacking sequences are identified in the table.

We observe that any of the O layers in the listing (1) can be chosen as the initial alumina layer. This layer must be translated to an A site, which can be achieved by cyclic permutations. For the C sites to be translated to A sites we need one cyclic permutation, while for B sites to be translated to A sites we need two. All other sites are relabelled accordingly. For example, for $C \rightarrow A$, we have $A \rightarrow B$ and $B \rightarrow C$. For the Al positions the corresponding relabelling has to be performed, keeping the subscripts [α (1), ...] fixed.

Next, we note that reflections about the xz plane [$\Leftrightarrow$ (010)] or yz plane [$\Leftrightarrow$ (100)] are symmetries of bulk

Table 2. Mapping of stacking and site labels (as defined in figure 1) under mirror transformations. A reflection about the xz plane leads, for example, to a relabelling of $c_\beta \rightarrow c_\gamma$.

Reflection about	Effect on					
	$A(a)$	$B(b)$	$C(c)$	$\alpha(1)$	$\beta(2)$	$\gamma(3)$
xz plane	$A(a)$	$B(b)$	$C(c)$	$\alpha(1)$	$\gamma(3)$	$\beta(2)$
yz plane	$A(a)$	$C(c)$	$B(b)$	$\alpha(1)$	$\beta(2)$	$\gamma(3)$

alumina. Although the structure is not invariant under these transformations, the transformed structures are equivalent to the original one. Table 2 lists the effects of mirror transformations in α- and κ-Al_2O_3 on individual stacking sites.

The fixed stacking sequence of the TiC substrate breaks the symmetry associated with a reflection about the yz plane. Such a reflection corresponds to interchanging $C \leftrightarrow B$ and $c \leftrightarrow b$. Hence, for each alumina sequence, we need to consider an additional one, which is obtained by interchanging $B(b) \leftrightarrow C(c)$.

Finally, we exploit that reflection about the xz plane is still a symmetry of TiC/alumina since the TiC is composed of fully occupied layers. Hence, alumina sequences that are related by $\beta \leftrightarrow \gamma$ ($2 \leftrightarrow 3$) are equivalent, see table 2.

For α-Al_2O_3, all O layers are equivalent. Therefore it is sufficient to focus on the first O layer, which is already in A stacking. Also, $\alpha[001] \Leftrightarrow \alpha[00\bar{1}]$ and thus only the symmetry breaking associated with the reflection about the yz plane needs to be considered. As a result, only two possible interfacial configurations have to be taken into account (see table 1, left column).

For κ-Al_2O_3, only every second O layer is equivalent and κ[001] is not equivalent to $\kappa[00\bar{1}]$. Therefore, we need to consider both directions, any two consecutive bulk O layers, and the effect of the symmetry breaking. This results in four different configurations for each direction (see table 1, middle and right columns).

3.2. TiC/thin-film alumina candidate structures

We obtain a pool of initial thin-film alumina geometries in three steps. First, we truncate the TiC/alumina interface sequences in table 1 after a full Al layer. The number of O layers n defines the thickness of the film. Second, the resulting configurations are distorted by placing the Al sublayers into one and the same plane, exactly in between the two neighbouring O layers. Third, we vary the stoichiometry by removing Al ions from the surface in accordance with the bulk space group, i.e. only Al pairs that belong to the same stacking label are removed.

In this way, for each thickness, we generate films with three different stoichiometric compositions: $Al_{4n}O_{6n}$, $Al_{4n-2}O_{6n}$ and $Al_{4n-4}O_{6n}$, corresponding to the removal of zero, one and two Al pairs, respectively.

We stress that the different stoichiometric compositions all approach the full Al_2O_3 stoichiometry in the limit of very thick films. Thus, for thick films, the different composition classes differ only in the details or nature of the nucleation[8]. We use the detailed notation to precisely discriminate between different possibilities for the alumina film nucleation.

Further details on the considered initial thin-film candidates such as choices for the location of surface Al, unrelaxed stacking sequences and the relative energies after relaxations are listed in the supplementary materials (available at stacks.iop.org/JPhysCM/22/015004/mmedia).

4. The *ab initio* method

4.1. Total energies and atomic relaxations

All calculations are performed with the DFT plane-wave code DACAPO [24] using ultra-soft pseudopotentials [25] and the PW91 exchange–correlation [26] functional.

We use a supercell approach and model the TiC/thin-film alumina by slab geometry. The basal plane dimensions of the supercell are chosen to fit the 3 × 2 TiC(111) surface (5.306×9.190 Å^2) and the height is fixed to 30 Å, ensuring a vacuum thickness of at least 13 Å.

The TiC is modelled by four atomic bilayers (with six Ti and six C atoms per bilayer). The alumina films contain six O atoms per O layer and a varying number of Al atoms, depending on the film stoichiometry. In total, the slabs contain between 64 (Al_4O_{12} films) and 86 atoms ($Al_{14}O_{24}$ films).

We use a 400 eV plane-wave cutoff and a 4 × 2 × 1 Monkhorst–Pack [27] k-point sampling. Electrostatic effects arising from the charge asymmetry in the slab are corrected for by a dipole correction. The atomic relaxations are performed until all interatomic forces are smaller than 0.05 eV Å^{-1}. This choice has proven a good accuracy at acceptable CPU times for α- and κ-Al_2O_3 surfaces [17] and for TiC/alumina interface calculations [28]. The presented DFT calculations amount to a total of one million CPU hours on modern supercomputing facilities.

4.2. Ab initio equilibrium thermodynamics

At non-zero temperature T and pressure p the stability of any system is governed by the Gibbs free energy G. For example, for a gas like O_2, the Gibbs free energy is given by the chemical potential μ_{O_2} which can be expressed in the ideal gas approximation by

$$\mu_{O_2}(T,p) = \epsilon_{O_2}^{\mathrm{DFT}} + \Delta\mu_{O_2}(T,p) = \epsilon_{O_2}^{\mathrm{DFT}} + \delta\mu_{O_2}(T,p_0) + k_B T \ln\frac{p}{p_0}, \qquad (2)$$

using DFT to determine the internal energy $\epsilon_{O_2}^{\mathrm{DFT}}$. In equation (2), $\delta\mu(T, p_0)$ is related to the entropy S and enthalpy H of O_2 at a fixed pressure p_0. The function $\delta\mu(T, p_0)$ can be obtained from tabulated values of $S(T)$ and $H(T)$ for different temperatures at standard pressure $p_0 = 1$ atm, see, e.g., [29].

Surface or interface free energies, σ or γ, are essentially defined as the difference between the free energy of the system that represents the surface or interface and the free energy of each of its constituents. Figures 2(a) and (b) show typical atomic set-ups using slab geometry to calculate the Gibbs free energies [30, 31]. In both cases two surfaces or interfaces are introduced and only the sum of their free energies, that is, $2\sigma_{\mathrm{av}} = \sigma^+ + \sigma^-$ or $2\gamma_{\mathrm{av}} = \gamma^+ + \gamma^-$, can be calculated. For a symmetric slab, we have, however, $\sigma = \sigma_{\mathrm{av}} = \sigma^+ = \sigma^-$ and correspondingly for γ. In that case, we have

$$\sigma \text{ or } \gamma = \frac{1}{2A}\Big(G_{\mathrm{slab}} - \sum_{i\in\mathrm{slab}} n_i\mu_i\Big), \qquad (3)$$

where G_{slab} is the Gibbs free energy of the total slab, i identifies all atomic constituents in the slab, μ_i is the corresponding chemical potential and A is the surface or interface area.

References [11–13] have developed a standard implementation for calculating the surface or interface Gibbs free energies of X_nO_m oxides and for relating these free energies to the temperature and O_2 pressure of a surrounding environment. The three essential ingredients are (i) the equilibrium condition between the surface or interface atoms with bulk atoms:

$$n\mu_X + m\mu_O = g_{X_nO_m}, \qquad (4)$$

where $g_{X_nO_m}$ denotes the Gibbs free energy per stoichiometric unit of the bulk material, (ii) the assertion that the Gibbs free energy of the solid material (bulk or slab) can essentially be replaced by its total energy E_{tot}[9] and (iii) the assumption that the oxide is in equilibrium with the O_2 of the surrounding environment, that is

$$\mu_O(T,p) \equiv \tfrac{1}{2}\mu_{O_2}(T,p), \qquad (5)$$

with μ_{O_2} evaluated as in (2).

Figure 2(c) illustrates the atomic set-up we are using for the thin films. The stability of such a system is governed by the surface stability of the film (σ), the stability of the interface between the substrate and the film (γ) and the stability of the

[8] Another way to think of the different stoichiometries is to focus on their surface termination: $Al_{4n}O_{6n}$ ⇔ Al_4-terminated, $Al_{4n-2}O_{6n}$ ⇔ Al_2-terminated and $Al_{4n-4}O_{6n}$ ⇔ O-terminated. However, the surface termination is not necessarily conserved after relaxations.

[9] While the Gibbs free energy of solids is almost independent of the pressure, the temperature dependence is not necessarily small. Based on the calculated vibrational surface Gibbs free energy for RuO_2 [13], we estimate the vibrational Gibbs free energy per cell for alumina at $T = 1000$ K as $\Gamma^{\mathrm{vib}} \sim$ 1–2 eV. However, we will show that the different Γ for different stoichiometric film compositions are of the order of 5–10 eV in the largest range of the most interesting region of the O chemical potential. Moreover, although small regions, where these differences become of the order of Γ^{vib} exist, we have to keep in mind that it is not the absolute value of Γ^{vib} but rather the differences in Γ^{vib} for different surface terminations that determine the stability. These can be expected to be considerably smaller than the absolute value of Γ^{vib}. Hence, the only effect of neglecting vibrational contributions is a small uncertainty in the value of μ_O which divides regions where different stoichiometries are stable.

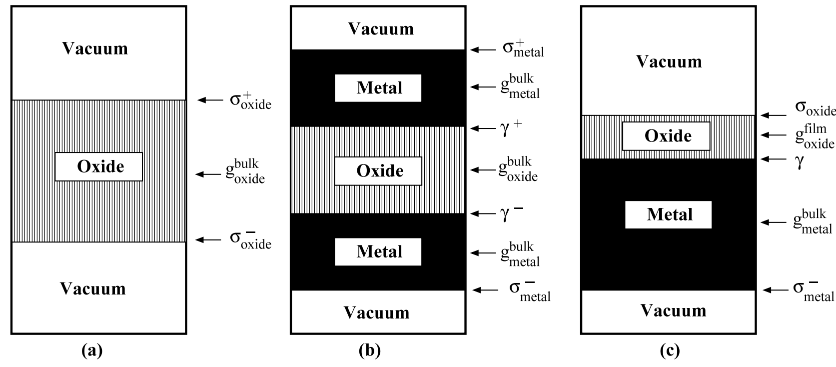

Figure 2. Schematics of atomic set-up for calculations of (a) (oxide) surfaces, (b) (metal/oxide) interfaces and (c) thin-film oxide on a metal substrate. The arrows point to the regions in the slabs where the bulk (g^{bulk}), surface (σ), interface (γ) or thin-film (g^{film}) contributions to the Gibbs free energy are located. We emphasize that, in general, $g^{bulk}_{oxide} \neq g^{film}_{oxide}$.

film itself ($g^{film}_{Al_2O_3}$). The stability of the system is therefore conveniently described by

$$\Gamma = A(\gamma + \sigma - \sigma^-_{TiC} - 2\sigma^+_{TiC}) = E_{TiC/Al_nO_m} - E_{TiC} - n_{Al}\mu_{Al} - n_O\mu_O, \quad (6)$$

where we have omitted a normalization by the surface area.

We note that the equilibrium condition in (4) is problematic for a thin oxide film. The Gibbs free energy per stoichiometric unit of an oxide in thin-film geometry may substantially differ from the Gibbs free energy per stoichiometric unit of the bulk, that is

$$g^{film}_{Al_2O_3} = g_{Al_2O_3} + \delta \neq g_{Al_2O_3}. \quad (7)$$

Here, δ measures the difference in Gibbs free energy between one stoichiometric unit in the bulk and in thin-film geometry. Although an exact value of δ cannot be calculated, we can estimate δ by calculating energy differences between films that differ by an integer number of stoichiometric units:

$$\delta_{nm} = (E_{Al_nO_m} - E_{Al_{n-4}O_{m-6}} - 2\epsilon_{Al_2O_3})/2. \quad (8)$$

We find that δ_{nm} is 0.4 and 0.7 eV when comparing three- and two-, and four- and three-layer thick films for $Al_{4n-4}O_{6n}$ stoichiometry. For $Al_{4n-2}O_{6n}$ stoichiometry the corresponding values are 0.3 and 1.2 eV. For $Al_{4n}O_{6n}$ stoichiometry we have only considered three-and two-layer thick films for which we find $\delta_{nm} = 1.1$ eV.

The fact that the largest values of δ_{nm} are found when calculating the energy differences for the thickest considered films is counterintuitive. We would expect that the difference in Gibbs free energy per stoichiometric unit converges towards that of the bulk once the film is thick enough. This shows the difficulties in determining the Gibbs free energy of a thin film properly. The higher values for thicker films may be due to completely different surfaces of the respective films and thus due to surface energies.

In the following, we disregard the fact of a non-zero value and the stoichiometry and thickness dependence of δ, that is, we put $\delta \equiv 0$. We have checked, however, that our results are qualitatively unchanged as long as the temperatures are not too high (below 1300 K).

The measure that determines the stability of our thin films is consequently given by

$$\Gamma \equiv E_{TiC/Al_nO_m} - E_{TiC} - \frac{n_{Al}}{2}\epsilon_{Al_2O_3} - \left(n_O - \frac{3}{2}n_{Al}\right)\mu_O, \quad (9)$$

where E_{TiC/Al_nO_m}, E_{TiC} and $\epsilon_{Al_2O_3}$ are DFT total energies of a TiC/Al_nO_m slab, an isolated (clean) TiC slab and one stoichiometric unit of bulk alumina, respectively.

Finally, the physically allowed range of chemical potentials are set as in the standard implementation of thermodynamical stability analysis for oxides by Al condensation into fcc Al and O condensation into O_2. It therefore follows that $\mu_{Al} < g_{fcc-Al}$ and $\mu_O < \frac{1}{2}\mu_{O_2}$, where g_{fcc-Al} and μ_{O_2} are the Gibbs free energy per stoichiometric unit of fcc Al and the chemical potential of O_2, respectively. Combining both inequalities and the equilibrium condition yields

$$\tfrac{1}{3}(g_{Al_2O_3} - 2g_{fcc-Al}) < \mu_O < \tfrac{1}{2}\mu_{O_2}. \quad (10)$$

In practice, the oxygen chemical potential μ_O is given by (5).

5. Results

A full list of unrelaxed stacking sequences of all candidate configurations, their energetics after relaxation and a discussion of the problems in relating these two can be found in the supporting material (available at stacks.iop.org/JPhysCM/22/015004/mmedia).

Apart from the stable (lowest energy) thin-film geometries, we also put an emphasis on potentially metastable configurations in the analysis of favourable structural motifs. Metastable here means that the relative energy of the configuration, $E_{rel} = E - E_0$, where E is the total energy of the configuration and E_0 is the total energy of the energetically lowest-lying configuration with the same stoichiometric composition, is below a certain value, $E_{rel} \lesssim E_{meta}$. We define E_{meta} in terms of the energy difference between the stable bulk α-Al_2O_3 and the metastable bulk κ-Al_2O_3. In our calculations we find a value of $\Delta_{\alpha\kappa} \sim 0.07$ eV/Al_2O_3 for this difference. An indicative measure of a potential metastability of the alumina films is thus given by $E_{meta} = 2n\Delta_{\alpha\kappa}$, where n is again

the number of O layers in the alumina film. For stoichiometric films, $2n$ is equal to the number of stoichiometric Al_2O_3 units in the film. For non-stoichiometric films, it serves as an approximate measure of the number of stoichiometric units.

5.1. Trends in phase content, orientation and preferred stacking

In the supplementary materials (available at stacks.iop.org/JPhysCM/22/015004/mmedia), we identify trends in relations between unrelaxed alumina structures and their energies after relaxation. Here we only list these trends:

- The stable and metastable alumina films are in general obtained by relaxing truncated TiC/κ-$Al_2O_3[00\bar{1}]$ interface configurations.
- For unrelaxed structures that differ only by a reflection about the yz plane, those that possess an AC stacking in the bottom two O layers yield more favourable thin-film geometries upon relaxation than those with AB stacking in the bottom two O layers.

We note that several important exceptions to these trends occur for $Al_{4n-2}O_{6n}$ films, and modifications can result in the energetically most favourable structure. For example, for $n = 2, 3$, α-Al_2O_3-derived films reach (meta-) stable relaxed configurations. Furthermore, for $n = 3, 4$, the stable films possess an AB stacking in the bottom two O layers.

5.2. Thermodynamical stability

The top panel of figure 3 shows our calculated values of Γ for the energetically most favourable configurations of each considered alumina thickness and stoichiometry class. The bottom panel of figure 3 shows the relation between the O chemical potential and the O_2 pressure at several temperatures.

In the physically interesting range, that is, for temperatures below $T \sim 1300$ K (upper limit for CVD temperatures) and O_2 pressures above $p_{O_2} \sim 10^{-15}$ bar (ultra-high vacuum), TiC/$Al_{4n-4}O_{6n}$ is predicted to be stable. For higher temperatures and/or lower O_2 pressures TiC/$Al_{4n-2}O_{6n}$ may become stable[10].

5.3. Atomic structure of the $Al_{4n-4}O_{6n}$ films

We note that, in general, the potentially metastable $Al_{4n-4}O_{6n}$ films, if present, possess the same atomic structure as the energetically most favourable film but rotated by 180° around the TiC[111] direction [$B \leftrightarrow C, \beta(2) \leftrightarrow \gamma(3)$]. They are therefore not discussed in the following.

Two-O-layer-thick films—Al_4O_{12}. The top left panel in figure 4 reports the calculated atomic structure of the energetically most favourable Al_4O_{12} film. It is noticeable that the O–O separation in the alumina is relatively large, $d_{O-O} \sim 2.6$ Å on average. Also, the two Al pairs are not located between the O layers but are almost incorporated in the surface O layer, which leads to a large splitting of that layer. At the same time, the Ti–O separation is comparably small and equals that in TiC/O.

Hence, although predicted to be stable in a thermodynamical sense, structurally this TiC/Al_4O_{12} configuration separates

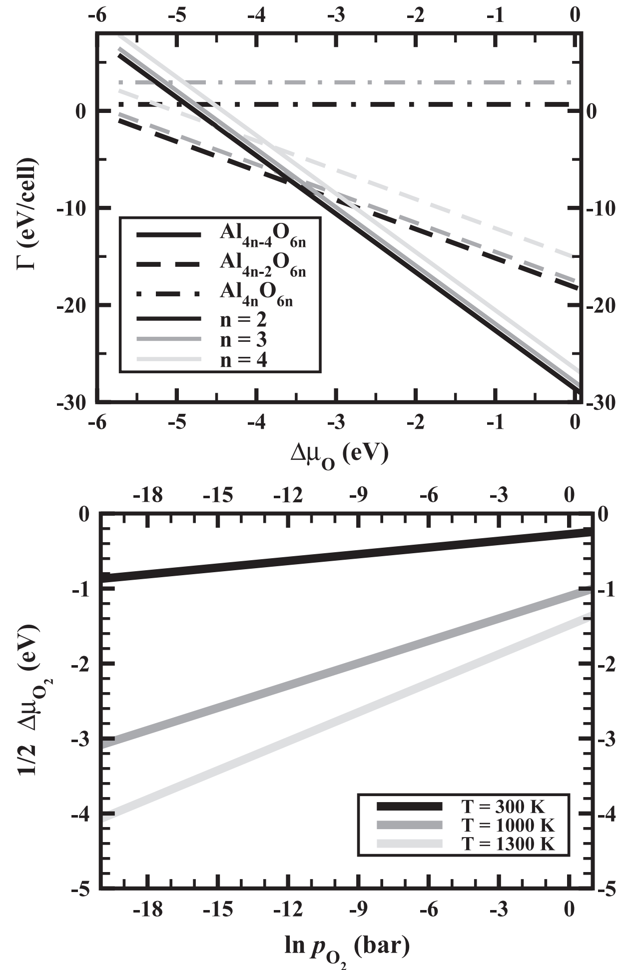

Figure 3. Thermodynamic stability of thin-film alumina with stoichiometrically different compositions and different thicknesses on the TiC(111) substrate, evaluated under the assumption of equilibrium with an O_2 environment. The top panel shows the Gibbs free energy differences Γ (see (9)) per unit cell of TiC/thin-film alumina for all three considered thicknesses and stoichiometric compositions as a function of the O chemical potential $\Delta\mu_O \equiv \mu_O - \frac{1}{2}\epsilon_{O_2}^{DFT}$ ($\Delta\mu_O = 0$ corresponds to O_2 formation). The left end of each line is defined by the physically allowed range (fcc Al condensation) of the O chemical potential (see (10)). For all thicknesses the alumina films with $Al_{4n-4}O_{6n}$ stoichiometry (solid lines) are stable at medium to high O chemical potential, whereas films with $Al_{4n-2}O_{6n}$ stoichiometry (dashed lines) are stable at low O chemical potential ($\Delta\mu_O < -3.5$ eV). The alumina films with $Al_{4n}O_{6n}$ stoichiometry (dashed–dotted lines) are not stable at any allowed value of the O chemical potential. The bottom panel shows one-half of the O_2 chemical potential $\Delta\mu_{O_2}$ as a function of partial O_2 pressure for three different temperatures. The standard implementation of thermodynamical stability analysis for oxides assumes that $\Delta\mu_O \equiv \frac{1}{2}\Delta\mu_{O_2}$, see (5).

[10] By including a thickness-and stoichiometry-dependent value of δ we find that the $Al_{4n-4}O_{6n}$ films are still stabilized down to $\mu_O \geqslant -2$ to -2.5 eV, where the higher value applies for the thickest and the lower for the thinnest films. An O chemical potential of $\Delta\mu_O \geqslant -2$ eV is reached for considerably higher O_2 pressures (e.g. $T \sim 1300$ K, $p_{O_2} \sim 10^{-4}$ bar). However, we note that the estimate of δ for the thicker films may be too large, so that the resulting value of Γ is too low and the value of the O chemical potential $\Delta\mu_O \geqslant -2$ eV is too high. In any case, at not too high temperatures and not too low pressures, the $Al_{4n-4}O_{6n}$ stoichiometries will always be stabilized.

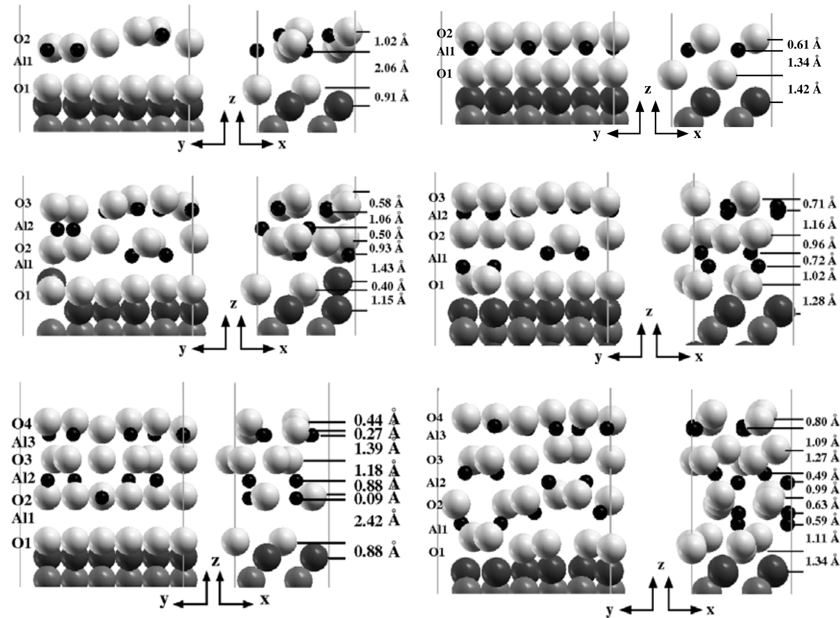

Figure 4. Side view on atomic structures of relaxed stable $Al_{4n-4}O_{6n}$ (left column) and $Al_{4n-2}O_{6n}$ (right column) films on TiC(111) for three different thicknesses ($n = 2, 3, 4$ (from top to bottom)) illustrating favourable structural motifs of thin alumina films. Colour coding: O = light grey, Al = black, Ti = dark grey, C = grey. In general the atoms are strongly distorted from ideal bulk sites. We note that these distortions always occur pairwise symmetrically in each sublayer. Left column: the TiC/$Al_{4n-4}O_{6n}$ separate into TiC/O and $Al_{4(n-1)}O_{6(n-1)}$ overlayer for $n = 2, 4$. The binding between the two is weak which can be inferred from the strong Ti–O bond (short bond length) and the fact that there are no Al ions between the O monolayer in the TiC/O and the bottom O layer in the $Al_{4(n-1)}O_{6(n-1)}$. For $n = 3$ the system is covalently bonded together via the Ti defect between the bottom two O layers. Note that for $n = 4$ the film geometry is α-like due to exclusively octahedrally coordinated Al ions. Right column: the binding in the TiC/$Al_{4n-2}O_{6n}$ system is considerably stronger, which is reflected by the increased Ti–O separation and the presence of Al ions between the bottom two O layers. Note the large number of tetrahedrally coordinated Al ions for $n = 3, 4$. More details about the stacking are listed in table 3 or can be found in the supplementary materials (available at stacks.iop.org/JPhysCM/22/015004/mmedia).

into a TiC/O/Al_4O_6 system, that is, a strongly bonded O monolayer on the TiC substrate with a thin stoichiometric alumina overlayer on top.

The stacking of the O layers is AC and the coordination of the Al ions is approximately $T_{\downarrow}O$[11].

Three-O-layer-thick films—Al_8O_{18}. The middle left panel in figure 4 shows the atomic structure of the energetically most favourable Al_8O_{18} film. The average O–O separation between the bottom two O layers is $d_{\text{O–O}} \sim 2.5$ Å, which is slightly shorter than the one in the stable Al_4O_{12} film. At the same time, the Ti–O separation is increased to 1.15 Å.

The stacking of the O layers is approximately ACA. In the middle O layer, the two O ions that should be located in C_β are, however, dislocated to cusp sites. Furthermore the whole surface O layer is strongly distorted from ideal sites. The coordination sequence of the Al ions is $T_{\downarrow}{:}OT_{\downarrow}T_{\downarrow}$.

Only one of the two original Al pairs is left between the bottom two O layers after relaxation. The other pair has moved in between the top two O layers. Interestingly, one of the interfacial Ti atoms has left the Ti layer and relaxed slightly in between the bottom two O layers. Again, structurally the TiC/Al_8O_{18} configuration appears as a partially decoupled TiC/O/Al_8O_{12} system. Here, however, the Ti impurity above the bottom O layer may be a stabilizing factor.

Four-O-layer-thick films—$Al_{12}O_{24}$. The bottom left panel in figure 4 shows the atomic structure of the stable $Al_{12}O_{24}$ film. The O stacking is $ACAB$ and hardly distorted. All Al ions have octahedral coordination. Thus, the present structure mixes the O stacking of bulk κ-Al_2O_3 with the Al coordination of bulk α-Al_2O_3.

The O–O separation $d_{\text{O–O}} \sim 2.5$ Å is again very large and the Ti–O separation is TiC/O-like. Also, one of the two original Al pairs in the bottom Al layer has relaxed upward through the middle Al layer and into the top layer. The other Al pair of the bottom layer is, after relaxation, located only 0.1 Å below the second O layer. Consequently, the TiC/$Al_{12}O_{24}$ configuration can also again be considered as a decoupled, weakly binding TiC/O/$Al_{12}O_{18}$ system.

5.4. Note on lattice mismatch between TiC(111) and alumina(001)

The surface-lattice mismatch between TiC(111) and α-Al_2O_3(001) is about 10%. One may therefore assume that, in our calculations, the alumina films are forced into a highly strained structure that could undergo atomic rearrangements if the strain is released. Furthermore, these unstrained structures could have binding properties that are different from those of the strained films.

[11] Here and in the following O denotes octahedrally coordinated Al pairs and T tetrahedrally coordinated pairs. For tetrahedral coordination, $T_{\uparrow}$ means that the tetrahedra point along the TiC[111] direction, away from the interface, whereas $T_{\downarrow}$ indicates that they point towards the interface. Different Al layers are separated by ‘:’.

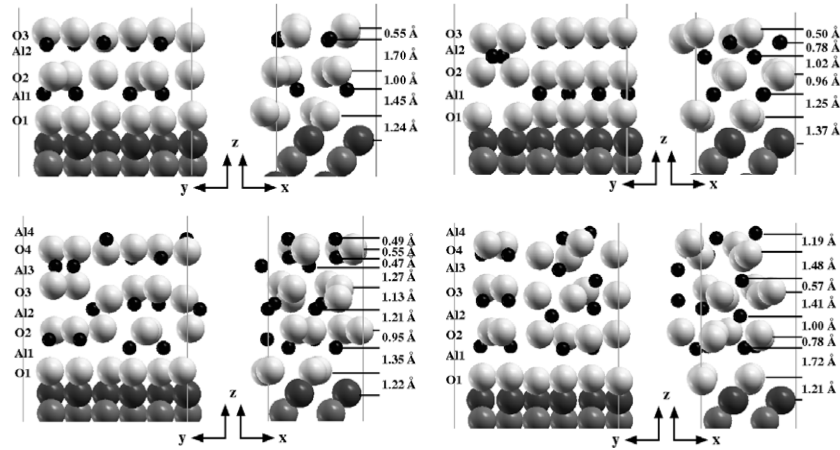

Figure 5. Side view of potentially metastable $Al_{4n-2}O_{6n}$ film geometries for $n = 3$ (top panels) and $n = 4$ (bottom panels) illustrating favourable structural motifs of thin alumina films. Colour coding: O = light grey, Al = black, Ti = dark grey, C = grey. Tetrahedrally coordinated Al ions dominate the second Al layer for $n = 3$. For $n = 4$, a partial $\kappa[00\bar{1}]$ geometry is recovered (bottom left panel). Also a geometry with non-symmetric relaxations of the Al ion is found (bottom right panel). The relative energies per unit cell, $E_{\rm rel}$, of the above films are (from left to right) 0.15 eV and 0.37 eV for the three-layers-thick films (for which we define a metastability limit by $E_{\rm meta} = 0.42$ eV), and 0.44 eV and 0.62 eV for the four-layers-thick films (for which we define a metastability limit by $E_{\rm meta} = 0.56$ eV). More details about the stacking are listed in table 3 or can be found in the supplementary materials (available at stacks.iop.org/JPhysCM/22/015004/mmedia).

The favourable TiC/$Al_{4n-4}O_{6n}$ configurations generally relax to stoichiometric alumina overlayers weakly binding to the O-passivated TiC surface. It is likely that the overlayers will relax to the α-Al_2O_3 lattice constant and form an incommensurate structure.

We have therefore performed calculations where we test the consistency of our description for TiC/$Al_{4n-4}O_{6n}$ systems. Specifically, we make two additional comparisons in which we (i) remove the TiC substrate but keep the lattice constant unchanged and (ii) remove the TiC substrate and adjust the lattice to the computationally optimized bulk α-Al_2O_3 lattice.

In the first case, hardly any relaxations take place and the difference between the unrelaxed (cut-out) and relaxed film is $\Delta E_{\rm relax} = 0.026$ eV/cell in favour of the latter. This result strengthens our observation that the interaction with the O-passivated TiC substrate is extremely weak. The organization of the overlayer results entirely from forces within the alumina.

In the second case, we find indeed stronger relaxations leading to a gain of $\Delta E_{\rm relax} = 0.44$ eV/cell with respect to the strained configuration. The relaxations result from the release of stress. Essentially only the film thickness increases (by 0.13 Å) which is expected due to the decreased in-plane surface cell. However, in all other respects, the two films, strained and unstrained, are identical in their geometry (available at stacks.iop.org/JPhysCM/22/015004/mmedia). With similar atomic arrangements it is unlikely that a significant change in the binding to the O-passivated TiC can arise.

In summary, we argue that, even if a unit cell large enough to fit both an unstrained TiC substrate and an unstrained alumina overlayer was obtained, the conclusion (that the binding between the two is extremely weak) would be unchanged.

5.5. Atomic structure of the $Al_{4n-2}O_{6n}$ films

Two-O-layer-thick films—Al_6O_{12}. The top right panel in figure 4 shows the atomic structure of the energetically most favourable Al_6O_{12}. It corresponds to a close-packed continuation of the TiC ABC substrate stacking, that is, the alumina stacking is $Ab_\alpha b_\beta b_\gamma C$. All Al ions share the same atomic plane and are octahedrally coordinated. The relaxed film is O-terminated. Compared to TiC/O (O monolayer on TiC(111)), the Ti–O layer separation is drastically increased (+0.5 Å).

The potentially metastable Al_6O_{12} structures possess almost the same structure as the energetically most favourable one. They differ only by a slight displacement along the z direction of some of the Al ions.

Three-O-layer-thick films—$Al_{10}O_{18}$. The middle right panel in figure 4 shows the atomic structure of the energetically most favourable $Al_{10}O_{18}$ film. Potentially metastable configurations are displayed in the top panels of figure 5. In all cases, the Ti–O layer separation is shorter than in the energetically most favourable Al_6O_{12} film, but still considerably larger than in TiC/O ($\sim +0.3$ Å). We also note that, in the stable $Al_{10}O_{18}$ film, two of the six O ions in the bottom O layer are slightly lifted off from the TiC substrate. In the potentially metastable films, no O ion is lifted off.

In all displayed films, the surface Al pairs have relaxed below the terminating O layer, so that the second Al layer consists of three Al pairs and the film is O-terminated.

The stacking of O layers is approximately described by ABA, $AB(AC)_{\rm bridge}$ and ACA for the energetically most favourable film and the two potentially metastable films, respectively. The order is only approximate because a number of O ions are significantly distorted from ideal sites (as defined by the underlying TiC substrate). They are often located in

bridge or cusp sites. This effect is most pronounced in the third O layer in the first potentially metastable film, which is entirely located in bridge sites.

Similarly, the Al ions often deviate from ideal sites so that their description in terms of the bulk stacking labels becomes cumbersome. However, these distortions always occur pairwise, that is, Al pairs that are related by a bulk stacking label are dislocated symmetrically. The candidate structures generally preserve this symmetry of the motifs of the bulk phases.

The coordination of the Al ions is described as $T_\uparrow T_\downarrow{:}T_\downarrow OO$, $OO{:}T_\downarrow T_\downarrow T_\downarrow$ and $OO{:}OT_\downarrow T_\downarrow$, for the energetically most favourable and the two metastable films, respectively.

We notice that, in all configurations, there is a large number of tetrahedrally coordinated Al ions (40–60%) and these can share the same atomic layer. In particular a larger number of tetrahedrally coordinated Al ions is favoured. Furthermore, the energetically most favourable film contains tetrahedrally coordinated Al ions that share one layer and for which the tetrahedra point in opposite directions.

Four-O-layer-thick films—$Al_{14}O_{24}$. The bottom right panel in figure 4 and the two bottom panels in figure 5 show the atomic structure of the energetically most favourable film and the two potentially metastable $Al_{14}O_{24}$ films, respectively. The Ti–O layer separations are comparable to those in the energetically favourable $Al_{10}O_{18}$ films. Also, in the stable $Al_{14}O_{24}$ film, two of the six O ions in the bottom O layer are slightly lifted off from the TiC substrate, whereas this is not observed in the potentially metastable films. In the most favourable film, the surface Al pairs have relaxed below the terminating O layer, so that the second Al layer consists of three Al pairs and the film is O-terminated. However, both potentially metastable films are Al-terminated even after relaxations.

The stacking of O layers is more strongly distorted as in the case of $Al_{10}O_{18}$ films, in particular in the most favourable film. From the figures (see also supplementary materials available at stacks.iop.org/JPhysCM/22/015004/mmedia), we find the approximate O stacking sequences $A(BC)_{\mathrm{bridge}}(A_\alpha A_\gamma C_\beta)B$ (the most favourable film, figure 4 bottom right panel), $ACBC$ (the first potentially metastable film, figure 5 bottom left panel) and $ABAC$ (the second potentially metastable film, figure 5 bottom right panel), where we use the labelling (subscript) of the Al positions also for O ions and note that some of the ions are, in fact, dislocated from ideal sites.

The Al ions are distorted correspondingly. This distortion is again pairwise and symmetrical for the energetically most favourable and the first potentially metastable films. For the second potentially metastable film, this is not true. Both on the surface and in the first and second layer below the surface there are Al ions that have relaxed in a non-symmetric way.

The coordination of the Al ions is given by $OT_\downarrow{:}T_\downarrow T_\uparrow{:}OT_\downarrow T_\downarrow$ (most favourable), $OT_\downarrow{:}OO{:}OT_\downarrow$ (first potentially meta- stable) and $T_\downarrow T_\downarrow{:}oT_\downarrow t_\downarrow{:}ooT_\downarrow$ (second potentially metastable). In the last sequence, the coordination of single ions that do not belong to a pair is denoted by lower-case letters (t, o). Also, the coordination of the surface Al ions is not given for the two potentially metastable films.

The result is similar to that for the $Al_{14}O_{24}$ films. In general, a large number of tetrahedrally coordinated Al ions is favoured. In the most favourable film 70% of the Al ions are tetrahedrally coordinated. Furthermore, there is a layer with purely tetrahedrally Al ions and tetrahedra pointing in opposite directions (second Al layer). The first potentially metastable film possesses only 30% tetrahedrally coordinated Al ions. Inspection of the detailed stacking sequence, $Ab_\beta a_\gamma Ca_\alpha a_\beta Bb_\beta a_\gamma Cb_\alpha$, identifies this structure as a partial κ-Al_2O_3 configuration with an orientation TiC[111]/κ[00$\bar{1}$].

6. Discussion

In section 5.1 we found that, although there are some general trends that relate initial unrelaxed alumina thin-film geometries with their energetics after relaxation, several important exceptions occur. These exceptions illustrate a potential danger of applying simple MC methods to the problem of finding the stable thin-film oxide structures. An importance sampling of the thin-film configuration space based on a classification of the unrelaxed structures in terms of, for instance, alumina phase content, orientation and/or O stacking may easily miss such exceptions.

These findings underpin the need for finding alternative approaches for structure search and motivate a discussion of the strategy that we have pursued.

6.1. Evaluation of structure-search strategy

We emphasize that the analysis of the relaxed stable and metastable thin-film geometries results in an identification of a number of new structural motifs that were not covered by the initial pool of motifs derived from bulk alumina. This finding of new structural motifs implies a significant strength and shows that the proposed structure-search strategy is not restricted to a sorting of the original candidate structures in an energetic order. The strategy is indeed capable of predicting energetically more favourable film geometries than what strictly constitutes symmetries in partial bulk structures.

We further note that we have used consistent assumptions about the pairwise symmetric placement of Al ions in our search strategy. In most of the energetically relevant relaxed thin-film geometries the detailed atomic positions deviate too strongly from ideal bulk positions to allow for a description in terms of the bulk stacking labels. However, the deviations in the Al placements always occur pairwise (with one exception for a metastable film, however). Al pairs that are related by a bulk stacking label in the unrelaxed configuration are relocated symmetrically to new positions that reflect the assumed underlying symmetry for Al pairs. Thus, the bulk symmetry associated with the mapping given in the lower panel of figure 1 is conserved in the films.

Table 3 implicitly lists the favourable structural motifs of thin films by summarizing the stacking of all stable and metastable thin-film alumina configurations in terms of the occupied O sites and Al coordination. For the $Al_{4n-4}O_{6n}$ films we find essentially only Al coordinations of the types OO and $OT_\downarrow$. The absence of

Table 3. Structure of energetically favourable thin-film alumina in terms of the O stacking (subscript label; A = fcc with respect to the TiC substrate, B = hcp and C = top) and approximate coordination of the Al ions (superscript label; O: octahedral, T: tetrahedral, the arrows indicate the direction in which the tetrahedra point; coordination of surface Al ions is unspecified). Favourable structural motifs can be identified as substructures of the full stacking.

n (# of O layers)	Favourable O stacking and Al coordination	
	$Al_{4n-2}O_{6n}$	$Al_{4n-4}O_{6n}$
2	$O_A\ Al^O\ Al^O\ Al^O\ O_C$	$O_A\ Al^O\ Al^{T_\downarrow}\ O_C$
3	$O_A\ Al^{T_\uparrow}\ Al^{T_\downarrow}\ O_B\ Al^O\ Al^{T_\downarrow}\ Al^O\ O_A$	$O_A\ Al^{T_\downarrow}\ O_C\ Al^O\ Al^{T_\downarrow}\ Al^{T_\downarrow}\ O_B$
	$O_A\ Al^O\ Al^O\ O_C\ Al^{T_\downarrow}\ Al^{T_\downarrow}\ Al^{T_\downarrow}\ O_A$	
	$O_A\ Al^O\ Al^O\ O_C\ Al^O\ Al^{T_\downarrow}\ Al^{T_\downarrow}\ O_A$	
4	$O_A\ Al^O\ Al^{T_\downarrow}\ O_B\ Al^{T_\uparrow}\ Al^{T_\downarrow}\ O_A\ Al^O\ Al^{T_\downarrow}\ Al^{T_\downarrow}\ O_C$	$O_A\ Al^O\ O_C\ Al^O\ Al^O\ O_A\ Al^O\ Al^O\ Al^O\ O_B$
	$O_A\ Al^O\ Al^{T_\downarrow}\ O_C\ Al^O\ Al^O\ O_B\ Al^O\ Al^{T_\downarrow}\ O_C\ Al$	

$OT_\uparrow$ is consistent with the fact that the stable configurations all derive from TiC/$\kappa[00\bar{1}]$ sequences (available at stacks.iop.org/JPhysCM/22/015004/mmedia). For the $Al_{4n-4}O_{6n}$ films we observe the domination of tetrahedrally coordinated Al. Whereas in the bulk, α-Al_2O_3 possesses 0% and κ-Al_2O_3 25% Al^T (all tetrahedra point along $\kappa[001]$), in the films this fraction may achieve values as high as 70% (stable $Al_{4n-2}O_{6n}$ configuration for $n = 4$). In detail, we find that layers with only tetrahedrally coordinated Al ions, $T_\downarrow T_\uparrow$ or $T_\downarrow T_\downarrow$, are energetically favourable, that layers with only octahedrally coordinated Al ions are present in both stable and metastable films and that Al layers with coordination $T_\uparrow T_\uparrow$ are not present.

A natural extension of the structure-search strategy could be obtained by including initial structures with a higher degree of tetrahedrally coordinated Al ions, in particular motifs such as $T_\downarrow T_\uparrow$ or $T_\downarrow T_\downarrow$. It is possible to cast this broadening of the initial network into the framework of a genetic algorithm for identifying surface reconstructions [32–34].

6.2. Note on the stability of CVD TiC/alumina wear-resistant coatings

We emphasize that a future, extended structure search for thin-film candidates is not expected to affect conclusions obtained by standard thermodynamical analysis of the stability of the various stoichiometric compositions of alumina films. Since the slopes of Γ in figure 3 (top panel) will remain unchanged, a possible identification of energetically more favourable structures in the two relevant stoichiometry classes will only resize the regions in which the different stoichiometries are stabilized. To make the $Al_{4n-4}O_{6n}$ films generally unstable in comparison to $Al_{4n-2}O_{6n}$ films, the truly stable $Al_{4n-2}O_{6n}$ configurations need to gain at least $\sim$10 eV/cell compared to the lowest-lying $Al_{4n-2}O_{6n}$ geometries identified in the present work. Thus, although the detailed atomic structure of the stable alumina film predicted here may differ from the detailed structure predicted by an extended search, the stable configuration can be expected to be of the type TiC/O/$Al_{4(n-1)}O_{6(n-1)}$.

At the same time we stress that the result that non- or weakly binding alumina films are thermodynamically favoured seemingly is in conflict with the wear resistance of TiC/alumina multilayers. We note, however, that the thermodynamic analysis is critically based on the present (standard) assumption of thermal equilibrium between the oxide films and an O_2 environment. During the formation of CVD TiC/alumina multilayers, alumina may never reach equilibrium with the surrounding O_2. In fact, extending the standard implementation of *ab initio* thermodynamics analysis to account for the actual CVD growth environment, we show in a forthcoming paper [35] that the strongly binding $Al_{4n-2}O_{6n}$ films are stabilized during CVD nucleation.

7. Conclusions

We present a strategy to sample the configuration space of possible thin-film structures of complex oxides on a substrate. A well-defined network of initial configurations for promising thin-film candidates can be designed from stable and metastable oxide bulk structures. *Ab initio* calculations of relaxation deformations provide candidates for thin films as a function of stoichiometry and oxygen-layer thickness.

The strategy has been illustrated for TiC/thin-film alumina, where experimental evidence [9, 14] can be used to reduce the network of initial thin films to contain structural motifs defined by bulk α- and κ-Al_2O_3. Based on this assumption, we have determined structural elements and candidates for the energetically most favourable (stable or potentially metastable) TiC/thin-film alumina configurations for three thicknesses and three stoichiometry classes.

The different stoichiometry classes have been compared by means of the Gibbs free energies. Based on the standard implementation of thermodynamics analysis, that is, by assuming equilibrium with an O_2 environment, we find that for the considered thicknesses of two, three or four O layers (corresponding to n = 2, 3 or 4, respectively), the stable films separate into an O-passivated TiC substrate and a non-binding stoichiometric $Al_{4(n-1)}O_{6(n-1)}$ overlayer. This finding (and the prediction that strongly binding alumina films ($Al_{4n-2}O_{6n}$ stoichiometry) are stable only at very high temperatures and in ultra-high vacuum) is in conflict with the wear-resistant character of TiC/alumina multilayers. In our discussion, we identify the equilibrium assumption in standard thermodynamics analysis as the origin of this discrepancy. This points towards a need to understand the detailed role of the environment during the nucleation of the films, a problem that will be discussed elsewhere [35].

Our *ab initio* structure-search strategy has proven predictive in the sense that it provides detailed insight into

the nature and atomic structure of thin-film alumina on TiC. The film geometries that are predicted by our method differ in their motifs heavily from motifs of the bulk, in particular in terms of the Al coordination. In principle, this warns us that the present implementation of the search may not yet be complete and that we cannot make an authoritative prediction of the stable thin-film alumina structure; we can at present only identify key structural elements. More importantly, this finding of additional favourable motifs documents its predictive power. It shows that the search strategy can identify candidate geometries with a nature that is not explicitly included in the network of initial configurations. The strategy can therefore be generalized in a natural way by iteration and inclusion of the structural motifs encountered in each iteration step.

Acknowledgments

The authors thank Sead Canovic and Mats Halvarsson for useful discussions. Support from the Swedish National Graduate School in Materials Science, from the Swedish Foundation for Strategic Research (SSF) through ATOMICS, from the Swedish Research Council (VR) and from the Swedish National Infrastructure for Computing (SNIC) is gratefully acknowledged.

References

[1] Levin I and Brandon D 1998 *J. Am. Ceram. Soc.* **81** 1995
[2] Haines J and Leger J M 1993 *Physica* B **192** 233
Dewhurst J K and Lowther J E 1996 *Phys. Rev.* B **54** R3673
[3] Surnev S, Ramsey M-G and Netze F-P 2003 *Prog. Surf. Sci.* **73** 117
[4] Wang J, Li H P and Stevens R 1992 *J. Mater. Sci.* **27** 5397
[5] Stierle A, Renner F, Streitel R, Dosch H, Drube W and Cowie B C 2004 *Science* **303** 1652
[6] Kresse G, Schmid M, Napetschnig E, Shishkin M, Khler L and Varga P 2005 *Science* **308** 1440
[7] Canovic S, Ruppi S, Rohrer J, Vojvodic A, Ruberto C, Hyldgaard P and Halvarsson M 2007 *Surf. Coat. Technol.* **202** 522
[8] Halvarsson M, Jonsson T and Canovic S 2008 *J. Phys.: Conf. Ser.* **126** 012075
[9] Halvarsson M, Nordén H and Vuorinen S 1993 *Surf. Coat. Technol.* **61** 177
[10] Rohrer J, Vojvodic A, Ruberto C and Hyldgaard P 2008 *J. Phys.: Conf. Ser.* **100** 082010
[11] Kaxiras E, Bar-Yam Y, Joannopoulos J D and Pandey K C 1987 *Phys. Rev.* B **35** 9625
[12] Batyrev I G, Alavi A and Finnis M W 2000 *Phys. Rev.* B **62** 4698
[13] Reuter K and Scheffler M 2001 *Phys. Rev.* B **65** 035406
[14] Halvarsson M, Trancik J E and Ruppi S 2006 *Int. J. Refract. Met. Hard Mater.* **23** 32
[15] Pauling L and Hendricks S B 1925 *J. Am. Chem. Soc.* **47** 781
Kronberg M L 1957 *Acta Metall.* **5** 507
Lee W E and Lagerlof K P D 1985 *J. Electron. Microc. Tech.* **2** 247
[16] Yourdshahyan Y, Ruberto C, Halvarsson M, Bengtsson L, Langer V and Lundqvist B I 1999 *J. Am. Ceram. Soc.* **82** 1365
[17] Ruberto C, Yourdshahyan Y and Lundqvist B I 2003 *Phys. Rev.* B **67** 195412
[18] Lee W E and Lagerlof K P D 1985 *J. Electron. Microc. Tech.* **2** 247
[19] Halvarsson M, Langer V and Vuorinen S 1995 *Surf. Coat. Technol.* **76–77** 358
[20] Halvarsson M 1994 *PhD Thesis* Chalmers University of Technology
[21] Ruberto C and Lundqvist B I 2007 *Phys. Rev.* B **75** 235438
Vojvodic A, Ruberto C and Lundqvist B I 2006 *Surf. Sci.* **600** 3619
[22] Dunand A, Flack H D and Yvon K 1985 *Phys. Rev.* B **31** 2299
[23] Oshima C, Aono M, Zaima S, Shibata Y and Kawai S 1981 *J. Less-Common Met.* **82** 69
[24] dacapo https://wiki.fysik.dtu.dk/dacapo
[25] Vanderbilt D 1990 *Phys. Rev.* B **41** 7892
[26] Perdew J P, Chevary J A, Vosko S H, Jackson K A, Pederson M R, Singh D J and Fiolhais C 1992 *Phys. Rev.* B **46** 6671
[27] Monkhorst H J and Pack J D 1976 *Phys. Rev.* B **13** 5188
[28] Ruberto C 2001 *PhD Thesis* Chalmers University of Technology
[29] Chase M W Jr 1998 *NIST-JANAF Thermochemical Tables* 4th edn (Gaithersburg: National Institute of Standards and Technology)
[30] Wang X-G, Chaka A and Scheffler M 2000 *Phys. Rev. Lett.* **84** 3650
Marmier A and Parker S C 2004 *Phys. Rev.* B **69** 115409
[31] Zhang W, Smith J R and Wang X-G 2004 *Phys. Rev.* B **70** 024103
[32] Chuang F C, Ciobanu C V, Shenoyb V B, Wanga C Z and Hoa K M 2004 *Surf. Sci.* **573** L375
[33] Sierka M, Todorova T K, Sauer J, Kaya S, Stacchiola D, Weissenrieder J, Shaikhutdinov S and Freund H-J 2007 *J. Chem. Phys.* **126** 234710
[34] Rohrer J and Hyldgaard P, unpublished
[35] Rohrer J, Ruberto C and Hyldgaard P, unpublished